Unlocking the Power of Resonance Raman Spectroscopy: the Case of Amides in Aqueous Solution

Sara Gómez[a], Franco Egidi[a], Alessandra Puglisi[a], Tommaso Giovannini[a], Barbara Rossi[b] and Chiara Cappelli[a,**]

[a]*Scuola Normale Superiore, Classe di Scienze, Piazza dei Cavalieri 7, 56126 Pisa, Italy.*

[b]*Elettra Sincrotrone Trieste S.C.p.A., S. S. 14 Km 163.5 in Area Science Park, I-34149, Trieste, Italy and Department of Physics, University of Trento, via Sommarive 14, I-38123 Povo, Trento, Italy.*

ARTICLE INFO

Keywords:
UV Resonance Raman
Fluctuating Charges
Amides
NMA
QM/MM

ABSTRACT

We report a joined experimental and computational study of Raman and Resonance Raman spectra of amides in aqueous solution. By employing state-of-the-art QM/MM methods combined with synchrotron–based UV Resonance Raman spectroscopy, we propose a protocol to interpret and reliably predict Resonance Raman spectra for amide systems in water, which are prototypical system for the peptide bond. We demonstrate that the main experimental spectral features can be correctly reproduced by simultaneously taking into account the dynamical aspects of the solvation phenomenon, specific solute-solvent hydrogen bond interactions and mutual solute-solvent polarization effects.

1. Introduction

Resonance Raman (RR) spectroscopy is a powerful tool to unveil structural and electronic properties of systems under different conditions. Much molecular information can be obtained from RR measurements, therefore numerous applications encompassing fields like analytical, physical and biophysical chemistry have been proposed.[1–4] Among the most experimentally studied systems using RR spectroscopy, are proteins[5–8], peptides[9–11], model peptides[12–19], aminoacids[20–22], (DNA) nucleobases[23–27] and a variety of inorganic compounds.[28, 29]

RR is a mixed electronic and vibrational spectroscopy, because it probes a system's vibrational degrees of freedom by employing an electromagnetic impulse which is in resonance with an electronic transition. Therefore, the approach combines the advantages of both types of techniques, i.e. the spectra can be directly connected to the vibrational degrees of freedom and thus structural aspects, while the ability to tune the spectra to a specific electronic transition can focus the signal on a single chromophore/portion of the system. Also, the ability to vary the wavelength of the probing laser permits to investigate the effect of the electronic transition upon the spectrum, enriching the description. Therefore, RR and especially UVRR, that provides selectivity and sensitivity through enhancement of particular vibrations associated to specific chromophores, has a very large potential.[30–33] However its full exploitation is hindered by the need for special experimental setups which are not as readily available as in the case of more common techniques. At the molecular level, through the resonance enhancement some selectivity is reached because the vibrational modes observed are only those whose motions couple to the electronic density change taking place in the electronic transition.[34, 35]

Evidently, the full exploitation of UVRR spectroscopy to selectively analyze vibrations in the system is contingent upon the experimental need of sources with appropriate characteristics of intensity, tunability and wavelength range extension. This is particularly critical in the case of deep ultraviolet (DUV) range of excitation (between about 150-300 nm), where lasers, which are widely used for visible Raman spectroscopy,[8, 36] suffer of some important limitations. The use of synchrotron radiation (SR) as source for UVRR experiments[37] appears to be an excellent choice because it offers advantages with respect to conventional laser sources. For instance, the possibility of extending the UV domain of excitation above 7 eV that would provide the chance to cover the whole range of outer electronic transitions in matter. In most laser-based UVRR studies, only a few discrete excitation wavelengths are used. The continuously tunability of SR enables a finely mapping of the whole resonance landscape of the sample in order to achieve a fine matching between the exciting radiation energy and the resonance conditions of specific chromophores. This allows to perform, for examples, accurate UVRR measurements not biased by self-absorption effects and/or to detect also the pre-resonance Raman scattered signal. Recently, the frontiers of UVRR spectroscopy were investigated by using synchrotron radiation, especially for the case study of investigation of peptides dissolved in their natural environment, i.e. aqueous solutions.[18]

Due to the complexity of information that is hidden behind RR spectral patterns (especially for aqueous systems), their interpretation benefits from the coupling with reliable theoretical simulations. Such calculations are generally doable for isolated systems, or systems in solution described by means of the Polarizable Continuum Model (PCM).[38–41] However, in general, substantial variations of the positions and relative intensities of the bands are observed after comparison with experimental spectra,[38, 40, 42] due to lack of any description of hydrogen bonding (HB) interactions. To get

*Corresponding author
chiara.cappelli@sns.it (C. Cappelli)
ORCID(s):

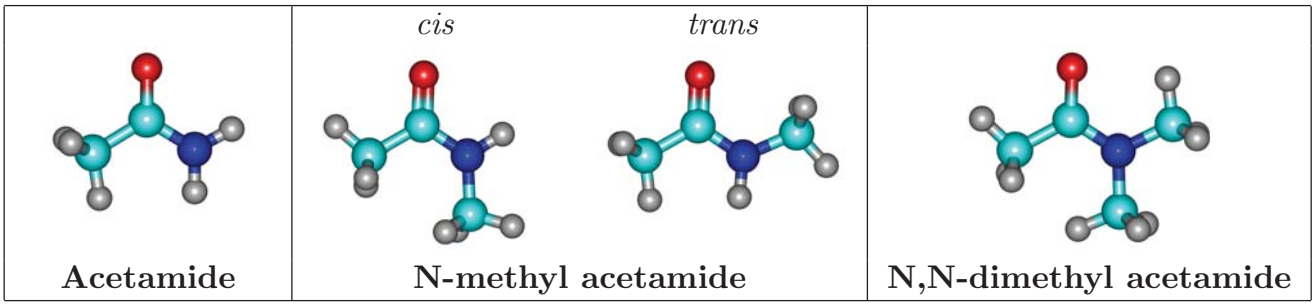

Figure 1: Structure of amides studied in this work. For NMA both *cis* and *trans* conformers are depicted.

over this limitation, researchers commonly resort to the so-called "cluster" methodologies, where explicit solvent molecules are included surrounding the potential hydrogen bond sites on the solute; and the entire system is then treated with Quantum Mechanical (QM) descriptions.[43, 44] Nevertheless, this procedure has its own weakness and not in all cases captures missing features.

As an alternative, a widespread practice is to split the entire system in layers to be treated at different model chemistries, with the part responsible of the property examined at the QM level and the rest computed at a much less expensive level of approximation, such as Molecular Mechanics (MM).[45, 46]

For the most part, QM/MM calculations of Raman spectra are oriented to the off-resonance (spontaneous) regime[46], whereas a few QM/MM applications to Resonance Raman spectra are available in literature.[47, 48] It is important to note that an atomistic description of the solvation shell only affects the spectroscopic properties of the solute directly, if it is polarizable, and is therefore able to dynamically respond to the probing electromagnetic field.[49] Therefore, in order to properly describe the physico-chemical nature of the solute-solvent interaction and how it affects the final spectrum, we resort to a polarizable QM/MM method based on fluctuating charges (FQ) known as QM/FQ,[50, 51] which has become a powerful tool to model a large variety of spectral signals of aqueous solutions.[49]

The aim of this work is to offer a detailed view of the effect of the solvation description on the simulation of Resonance Raman spectra of model peptides, by combining state-of-the-art theoretical techniques with an experimental setup based on SR radiation that allows us to fully exploit the potential of this technique. To this end, we extend QM/FQ for the first time to model RR, and we challenge it to reproduce experimental UVRR spectra of aqueous Acetamide (ACA), N-methyl acetamide (NMA), N,N-dimethyl acetamide (DMA) (see Figure 1). Such systems were not chosen by chance, rather they serve as models for the extensively documented peptide bond[30].

2. Methodology

2.1. QM/FQ approach to RR spectroscopy

The spontaneous Raman scattering cross-section is usually calculated at the DFT level using response theory by differentiating the dynamic electric polarizability with respect to the normal mode displacements, calculated for a perturbation with angular frequency ω corresponding to the one of the light source (e.g. a laser or synchrotron light). Given the vibrational transition polarizability α^i corresponding to an excitation of the i-th normal mode, then the cross-section σ_i can be expressed in terms of the Raman rotational invariants:

$$a_i^2 = \frac{1}{9}\sum_{ab}\alpha^*_{aa,i}\alpha_{bb,i} = \frac{1}{9}|\alpha_{xx,i} + \alpha_{yy,i} + \alpha_{zz,i}|^2 \quad (1)$$

$$g_i^2 = \frac{1}{2}\sum_{ab}(3\alpha^*_{ab,i}\alpha_{ab,i} - \alpha^{i*}_{aa,i}\alpha_{bb,i}) \quad (2)$$

$$\sigma_i = \left(\frac{\omega - \omega_i}{c}\right)^4 \frac{45a_i^2 + 7g_i^2}{45} \quad (3)$$

The harmonic approximation is usually invoked to describe the molecule's potential energy surface, and in the non-resonant regime the vibrational transition polarizability is expanded in a Taylor series to first order, and only the first derivative term is usually retained which is calculated either numerically or analytically. This method assumes that the imaginary part of the polarizability is negligible, which is true when the incident radiation is far-from-resonance, however in the resonant case the full sum-over-state expression must be considered

$$\alpha_{ab,i} = \frac{1}{\hbar}\sum_{m'}\frac{\langle i|\mu_a|m'\rangle\langle m'|\mu_b|0\rangle}{\omega_{m'} - \omega_i - \omega - i\gamma} \quad (4)$$

where the summation runs over all vibronic states belonging to the potential energy surface of the resonant electronic state, while γ is the excited state's phenomenological damping constant. This is the method used in this work to calculate the RR cross section, as detailed in Ref. 38. In particular, we employ the Vertical-Gradient, Franck-Condon approximation, where the vibrational frequencies and normal modes of the excited state are assumed to be the same as the ground state, and the transition dipole moments are considered to be independent of the molecular geometry.[38] The method employed to calculate the RR spectrum is considerably more involved compared to the one for spontaneous Raman, however it should be emphasized that attempting to simulate the Raman spectrum using the same methodology

employed in the non-resonant case by simply altering the incident frequency so that it is close to that of the electronic transition would lead to completely erroneous results, unless a method that explicitly includes the imaginary part of polarizability is used.[52]

The method employed in this work is also known as time-independent[38, 40] (TI) method, though an equivalent time-dependent[42, 53, 54] (TD) formulation has also been described. Calculations of vibrational Resonance Raman spectra of isolated and solvated molecules have been performed by resorting to these frameworks, combining different strategies for the description of the excited states,[24, 25, 31, 48, 55–58] though none have used a polarizable QM/MM model to include solvent effects in all terms within equation 4, to the best of our knowledge. The presence of the solvent must be carefully considered and included in all steps of the simulation.

In this paper, solvent effects are described by means of the FQ force field, in which each atom of the classical layer is endowed with a charge, whose value is not fixed, but is allowed to vary as a response to the electric potential produced by the QM density.[49] In recent years, the QM/FQ method has been extended to the calculation of analytical energy third derivatives, which allow for the calculation of spontaneous Raman spectra,[59] excitation energies,[60] and excited state gradients.[61] In equation 4 all terms include solvation effects evaluated at the QM/FQ level of theory: the ground state geometry of the molecule is first optimized in the presence of the solvent shell, then the electronic density and harmonic potential energy surface are modelled by taking the reaction field due to the water molecules into account. The contribution due to the water molecules also enters the response equations that are solved to calculate excitation energies and to model the excited state potential energy surface. Therefore, in order to properly simulate the RR spectrum of a system in solution, one requires a solvation method with the flexibility to model a wide array of molecular properties, involving both electronic and vibrational degrees of freedom, as well as excited states. In the last few years, the QM/FQ method has indeed been extended to the treatment of a vast set of spectroscopies, allowing us to finally tackle RR, which can be regarded as one of the most complex due to the interplay of all these features.[49–51]

3. Experimental procedure

Acetamide, N-methylacetamide and N,N-dimethyl acetamide were purchased by Sigma Aldrich and D.B.A. Italia and used without further purification. The aqueous solutions of the three molecules were prepared by dissolving ACA, NMA and DMA in high-purity water, deionized through a MilliQTM water system (>18 M cm resistivity), in order to obtain the desired molar fractions x (where x is defined as mole of solute/total number of moles of the solution) ranging from 0.2 to 0.01. It has been accurately checked that, at these values of concentration, the solutes are totally dissolved and the solutions appear limpid. All the samples were freshly prepared and placed into optical quartz cells for the Raman scattering measurements.

Out of Resonance Raman spectra were collected on the solutions of ACA, NMA and DMA by means of a micro-Raman setup (Horiba-JobinYvon, LabRam Aramis) in backscattering geometry and using the exciting radiation at 632.8 nm provided by a He-Ne laser. The resolution was set at about 1.2 cm^{-1}/pixel.

UV Resonance Raman (UVRR) measurements were collected at the BL10.2-IUVS beamline of Elettra-Sincrotrone Trieste (Italy)[37] using 210, 226 and 266 nm as excitation wavelengths. The exciting wavelength was set by adjusting the gap parameters of the undulator and by using a Czerny-Turner monochromator (Acton SP2750, Princeton Instruments) equipped with 1800 and 3600 grooves/mm gratings to monochromatize the incoming SR. The final radiation power on the samples was kept about 10-15 μW. The Raman scattered radiation was collected in back-scattered geometry and analyzed by using a single pass of a Czerny-Turner spectrometer (Trivista 557, Princeton Instruments). Depending on the excitation wavelength, the resolution was set between 1.8 and 2.8 cm^{-1}/pixel, in order to ensure enough resolving power and count-rate of the spectra. The calibration of the spectrometer was standardized using cyclohexane (spectroscopic grade, Sigma Aldrich). Any possible photo-damage effect due to a prolonged exposure of the samples to UV radiation was avoided by continuously spinning the sample cell during the measurements. The comparison between the individual spectra acquired for each sample evidences that no gradual changes to the spectra with respect to accumulation number were observed, confirming that any sample photodegradation due to UV exposure is not occurred in the experiments.

4. Computational details

All QM calculations were carried out at the B3LYP/aug-cc-pVDZ level of theory, using a locally modified version of the GAUSSIAN16 suite of programs.[62] Equilibrium geometries and ten vertical excitation energies of the three amides in water were obtained by using PCM to treat environmental effects.[41] For the three amides, CM5 point charges[63] were also calculated with the aim of using them in the Molecular Dynamics (MD) simulations.

Classical MDs were performed by using GROMACS 5.0.5 [64]. A single amide molecule (the most populated PCM conformer in the case of NMA (see Figure S1 in the Supplementary Material - SM) was inserted in a cubic box with an edge of 4.52 nm and solvated with around 3000 water molecules. In order to recover the correct directionality of solute-solvent hydrogen bonds, dummy atoms[65, 66] (virtual sites) were placed on the oxygen atom of the carbonyl group in each case,[65–69] specifically at the centroid positions, determined by the Boys localization procedure.[70] Bonding and non-bonding interactions were modeled according to the General Amber Force Field (GAFF).[71] After minimizing the energy of the solvated systems, a short (500 ps) simulation was performed at 298.15 K for thermalization

Journal Pre-proofs

purposes by adopting the canonical ensemble (NVT) with a velocity-rescale thermostat, and periodic boundary conditions applied in all directions. Production runs were performed in the isothermal–isobaric ensemble (NPT) by using the velocity-rescale method[72] with a coupling constant of 0.1 ps and a Berendsen barostat with time constant of 1.0 ps, saving coordinates every 10 ps. The total time of the simulation was set to 30 ns, with a time step of 2 fs. The MD trajectories were analyzed with the TRAVIS package.[73]

From the last 10 ns of the MD runs, 200 uncorrelated snapshots were extracted to be used in QM/FQ calculations, and for each of them, a sphere-shape of radius 15 Å centered on the solute molecule was cut. For each snapshot, the solute geometry was optimized at the QM/FQ level by keeping fixed the solvent molecules, by using the Berny algorithm.[74] On the optimized geometries, frequencies, excitation energies and excited state gradients were calculated as well. In all QM/FQ calculations, the FQ parametrization proposed in Ref. 75 was exploited. Note that the selected number of snapshots is sufficient to reach the convergence of the calculated spectrum (see Fig. S2 in the SM).

QM/PCM and QM/FQ spontaneous Raman spectra were computed in the dynamic regime by setting the incident frequency (ω_0) to match the experimental value of 633 nm, using analytical response theory as implemented for QM/FQ.[59] UVRR spectra were computed using a time-independent sum-over-state methodology.[38] In particular, we employed the Vertical Gradient Franck-Condon (VG|FC) approximation for the modeling of the excited-state Potential Energy Surface (PES) and transition dipole moments, by considering ten excited states (see also Fig. S3 in the SM). RR spectra were computed using an array of incident frequencies, producing Raman excitation profiles for all bands. Final QM/FQ UV/Vis and Raman, both spontaneous and RR, spectra were obtained by averaging the spectra from all the snapshots. For absorption spectra, Gaussian functions and a full width at half maximum (FWHM) of 0.65 eV were chosen, while spontaneous and RR sticks were convoluted with Lorentzian profiles and FWHM values of 8 and 20 cm^{-1}, respectively.

5. Results

Spectral features are often rationalized in terms of chromophores and functional groups. From this point of view the three amides considered in this work may appear very similar, however they present important structural and chemical differences that affect their intrinsic properties as well as their interaction with the aqueous environment. All three share the amide functional group characterizing their chemistry and can act as hydrogen bond acceptor through the non-bonding electron pairs of the carbonyl group (see Fig. 1). However they differ in the number of hydrogen atoms bonded to the amide nitrogen (those to be potentially donated to the water molecules), which changes the way they interact with the solvent, and this may strongly affect the resulting spectrum. In addition, NMA differs from the other two amides by virtue of *cis/trans* conformational freedom connected to the rotation of the NC bond, combined with the presence of two different moieties bonded to the nitrogen (see Fig. 1 and S1 in the SM). In this section, we first discuss the results obtained for trans NMA (i.e. the most stable conformer), followed by the other two systems. All spectral features are commented in terms of hydration patterns, as obtained from MD simulations. Notice that, because NMA is the simplest molecular model of the peptide linkage in proteins, it has motivated many experimental and theoretical studies[16, 76] with particular emphasis on solvent effects on RR spectra.[14, 43, 44, 77]

5.1. NMA

5.1.1. Spontaneous Raman spectra

Computed QM/PCM and QM/FQ spontaneous Raman spectra are shown in Figure 2(a) along with our own experimental Raman measurements. In Fig. 2(a), top panel, almost all QM/PCM bands for aqueous NMA are slightly narrower than QM/FQ (middle panel). This is due to the dispersion in the vibrational energies within the set of extracted snapshots (see Fig. S4 in the SM for QM/FQ raw data), and is a feature that is missing in a static model such as QM/PCM, which is based on calculations performed on a single minimum-energy structure.

The most relevant vibrational modes in the experimental NMA Raman spectra are amide I (1626-1646 cm^{-1}), amide II (1566-1584 cm^{-1}) and amide III (1313 cm^{-1}),[16, 17] which are all correctly reproduced by QM/FQ, which improves the description provided by QM/PCM, particularly in the regions where the strong amide bands are located (see Section S1.4 in the SM for a graphical depiction of the normal modes).

5.1.2. UV Resonance Raman spectra

UVRR spectra of aqueous NMA were measured by using 210, 226, and 266 nm as excitation wavelengths (ω_0), though the 266 nm-excited spectrum should be considered as pre-resonant because the probing wavelength is far from the maximum of the absorption spectrum (see Sec. S1.5 in the SM). The experimental UVRR spectrum collected by setting ω_0 =226 nm is graphically depicted in Fig. 2(b) (see Fig. S7 in the SM for UVRR spectra measured at different excitation wavelengths).

The value for the incident frequency to be exploited in both QM/PCM and QM/FQ calculations must perfectly reproduce the experimental conditions in order to preserve the resonance enhancement. Selecting the same ω_0, used for experimental measurements, would introduce systematic errors into the calculation because any electronic structure method carries some error in the description of electronic excited states which, within the frame of response theory, are obtained from the poles of the system's response function. Therefore, we follow the method described in 38, suitably adapted to QM/FQ calculations. In essence, we select a frequency that is at the same energy gap to the simulated absorption maximum as that observed experimentally (see Tab. S1 in the SM). QM/PCM and QM/FQ UVRR spectra are reported in Fig. 2(b).

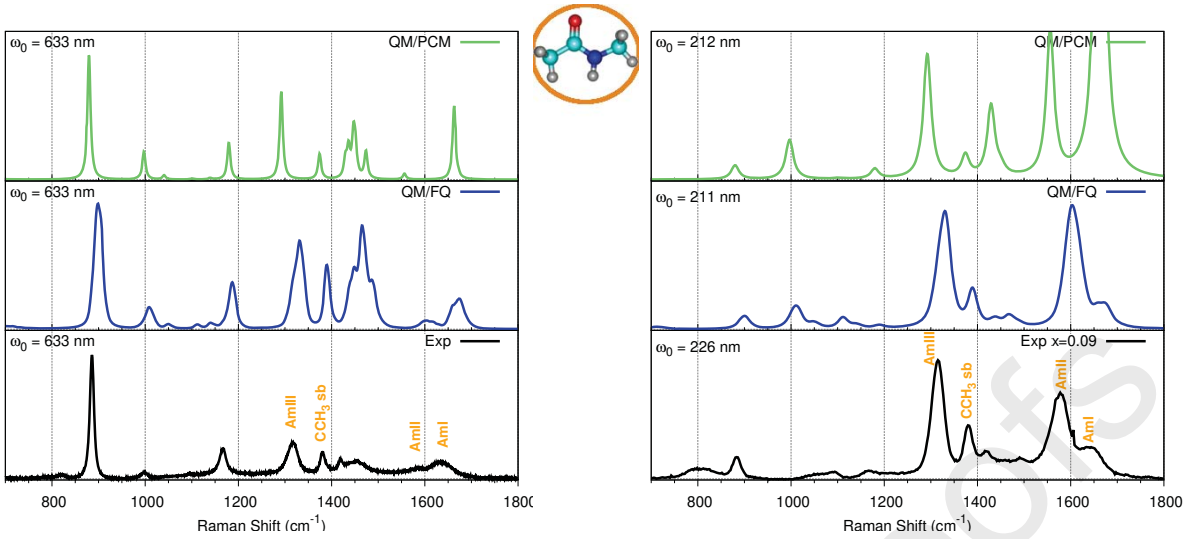

(a) (b)

Figure 2: Raman spectra of **NMA** calculated with different solvent descriptions and compared to experimental spectra measured in aqueous solution at room temperature. (a) Spontaneous (Far From Resonance) Raman spectra simulated and measured using 633 nm as excitation wavelength. FWHM: 8 cm^{-1}. (b) UV Resonance Raman spectra. In the UVRR experiments, the external excitation wavelengths have been set to 226 nm. x=0.09 is the NMA molar fraction in water. RR intensities were calculated with a damping factor of 200 cm^{-1} and broadened using Lorentzian functions with FWHM = 20 cm^{-1}. The RR band at around 800 cm^{-1} is a spurious signal arising from the quartz cuvette.

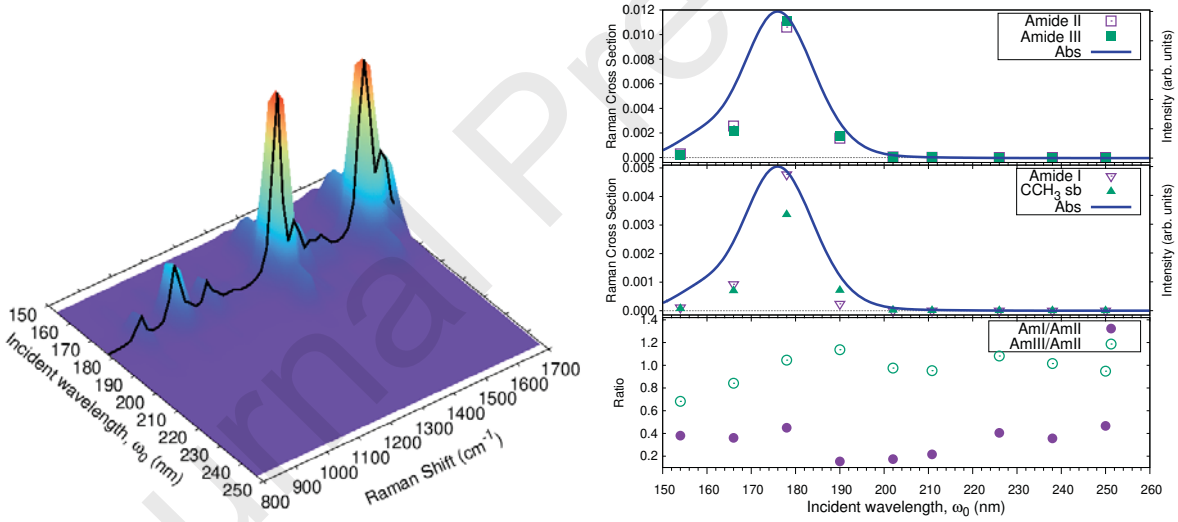

(a) (b)

Figure 3: (a) Calculated QM/FQ Resonance Raman Excitation Profiles (RREP) of **NMA** in aqueous solution. (b) Excitation wavelength dependence of the Amide I, II, III and the 1380 cm^{-1} CCH_3 symmetric bend (sb) band intensity, and of Amide I/Amide II and the Amide III/Amide II band Raman cross-section ratios. RR intensities (in $cm^2mol^{-1}sr^{-1}$) were calculated with a damping factor of 200 cm^{-1} and broadened using Lorentzian functions with FWHM = 20 cm^{-1}.

Comparing experimental UVRR and spontaneous Raman spectra in Fig. 2, different patterns can be highlighted: (*i*) a weaker or absent Amide I (C=O) stretching vibration (1626-1646 cm^{-1}), (*ii*) an enhancement of the signal involving C–N stretching, which is characteristic of Amide II (1566-1584 cm^{-1}), as well as the CH_3 umbrella bending (1380 cm^{-1}), (*iii*) an enhancement of the Amide III band (1313 cm^{-1}), gaining intensity relative to Amide I. [14, 16, 44, 76, 78] Such spectral features are perfectly reproduced by QM/FQ, which is for instance able to correctly predict smaller Amide I:Amide II intensity ratio when moving from off-resonant to resonant regime. Moreover, the atomistic approach outperforms QM/PCM in the description of most experimental bands. In fact, Amide I band is predicted as the strongest band in QM/PCM UVRR spectrum, and also, an overestimated enhancement for the methyl modes (peak erroneously emerging at 1440 cm^{-1}) is observed. The discrepancies between the QM/PCM and the experiment, together

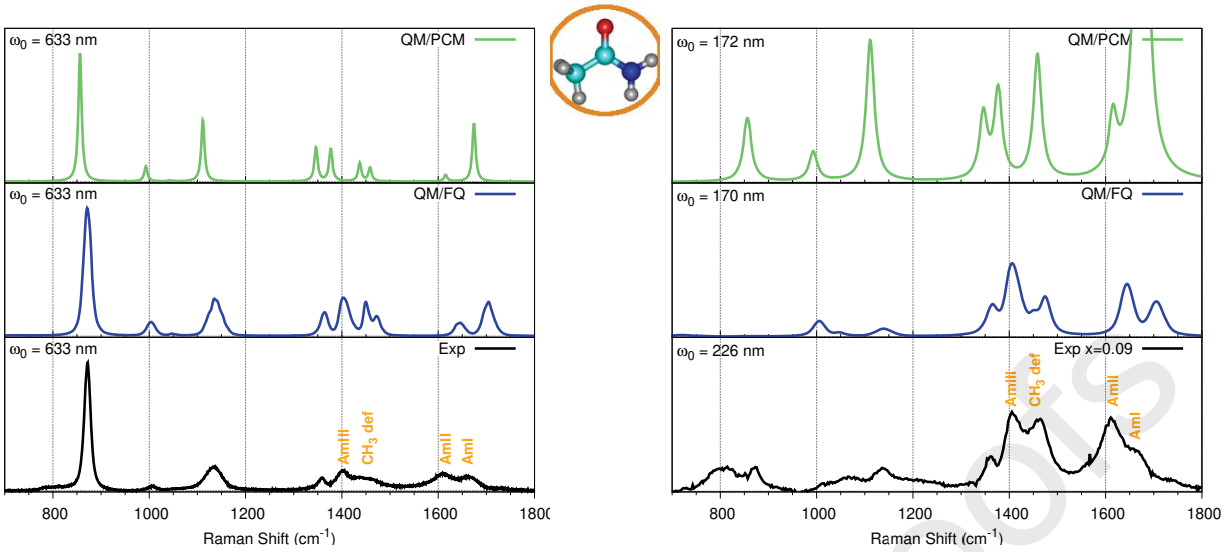

Figure 4: Raman spectra of **Acetamide** calculated with different solvent descriptions (top, QM/PCM and middle, QM/FQ) and compared to the experimental spectra (bottom) measured in aqueous solution at room temperature. (a) Spontaneous (Far From Resonance) Raman spectra simulated and measured using 633 nm as excitation wavelength. FWHM: 8 cm^{-1}. (b) UV Resonance Raman spectra. In the UVRR experiments, the external excitation wavelengths have been set to 226 nm. x=0.09 stands for the Acetamide molar fraction in water. RR intensities were calculated with a damping factor of 200 cm^{-1} and broadened using Lorentzian functions with FWHM = 20 cm^{-1}. The RR band at around 800 cm^{-1} is a spurious signal arising from the quartz cuvette.

with the almost perfect agreement provided by QM/FQ, clearly demonstrate the importance of specific solute-solvent interactions, appropriately coupled to a physically consistent treatment of polarization effects.

An aforementioned feature of the synchrotron-based UVRR setup is the ability to tune the excitation wavelength to obtain RR excitation profiles (RREP) for every band. In Fig. 3(b), computed QM/FQ RREP for NMA in aqueous solution are reported as 3D graphs where the Raman intensity is plotted as a function of both the incident wavelength (150 nm< ω_0 < 250 nm) and the Raman shifts. Sections of the 3D plots are shown in Figure 3(b), where we keep track of the enhanced Amide I, II and III peaks as well as the peak at 1380 cm^{-1} (CCH_3 symmetric bend - sb), which have been previously described. As expected, Figure 3 reveals that all the analyzed band excitation profiles present maxima around 178 nm, which corresponds to the vertical absorption of the $\pi \rightarrow \pi^*$ transition. We also note that Amide I/Amide II relative Raman cross-section ratios vary without any apparent trend in the studied wavelength range. However, amide I band is always weaker in intensity, in total contrast with QM/PCM results in Figure 2(b). Such findings also reveal that QM/FQ is notably able to account for the almost threefold enhancement of Amide II with respect to Amide I intensity that is experimentally measured.[76]

5.2. Acetamide

5.2.1. Spontaneous Raman spectra

QM/PCM and QM/FQ computed spontaneous Raman spectra of acetamide (ACA) in aqueous solution are reported in Fig. 4(a) together with their experimental counterpart measured by using ω_0 =633 nm.

We first notice that almost all peak relative intensities are correctly reproduced by both the solvation approaches, however the inhomogeneous broadening, and also the position of most bands, are better described by QM/FQ with respect to the implicit description. As in the case of NMA, in solvated acetamide, the amide I band located at 1662 cm^{-1} originates primarily from C=O stretching, whereas an amide II-like band occurs at 1616 cm^{-1} and is associated with NH_2 bending, even if contains a small contribution from C=O stretching (see Sec. S2.1 in the SM). The amide III-like band of ACA, located at 1404 cm^{-1} derives from the C-N stretching, but also has minor contributions of C-C stretching, NH_2 rocking, and symmetric deformations of the NCO group and CH_3 groups.[13]

Similarly to NMA, Amide I and Amide II bands are located in the region around 1600 cm^{-1}, where the broad H-O-H bending vibration of the water molecules contributes to the Raman intensity.[13, 79, 80]

5.2.2. UV Resonance Raman spectra

QM/PCM and QM/FQ UVRR spectra of ACA in aqueous solution are reported in Fig. 4(b), together with our spectra measured by using ω_0 =226 nm (see Fig. S10 in the SM for experimental UVRR measured with ω_0 =210, 226 and 266 nm). We first note that all experimental Raman peaks increase in intensity as the excitation wavelength decreases from 633 to 226 nm, with Amide I, II, and III bands showing the largest resonance enhancement, that in agreement with

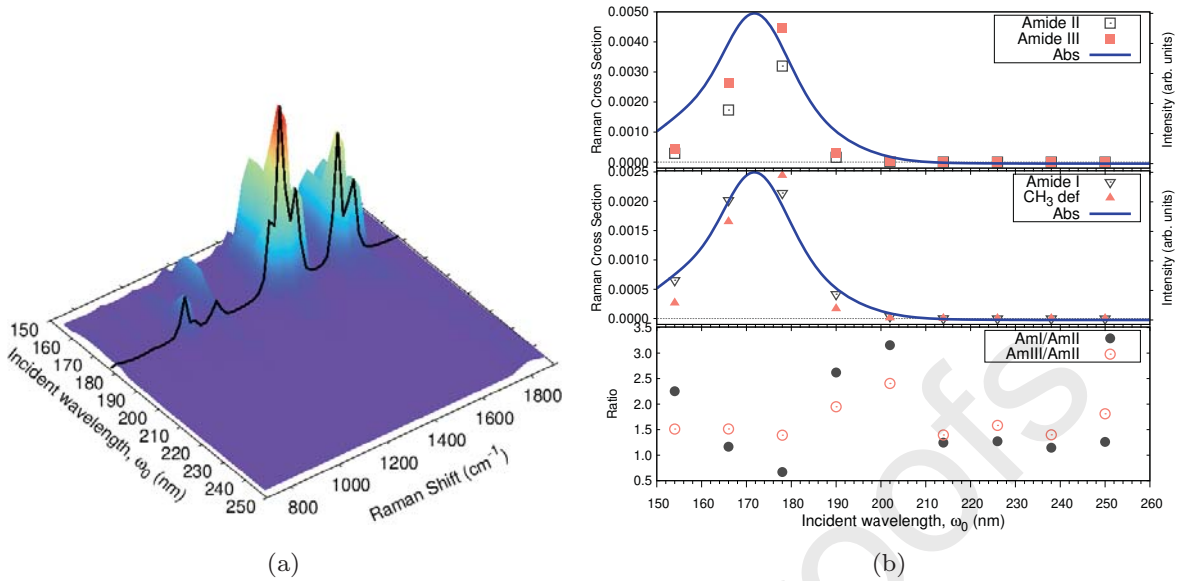

(a) (b)

Figure 5: (a) Calculated QM/FQ Resonance Raman Excitation Profiles (RREP) of **Acetamide** in aqueous solution. (b) Excitation wavelength dependence of the Amide I, II, III and and 1457 cm^{-1} CCH_3 deformation (def) bands intensity, and of Amide I/Amide II and the Amide III/Amide II band Raman cross-section ratios. RR intensities (in $cm^2mol^{-1}sr^{-1}$) were calculated with a damping factor of 200 cm^{-1} and broadened using Lorentzian functions with a FWHM of 20 cm^{-1}.

previous findings.[13] The same is valid for QM/FQ, which is able to provide an almost perfect agreement with the experiment in terms of relative intensities, band positions, and band broadening. Conversely, QM/PCM UVRR spectrum dramatically differs from the experimental counterpart. In particular, the amide I mode ($\sim 1700\ cm^{-1}$) is much more intense than in the experiments, similarly to what has been already commented for NMA. The nature of the normal mode, which is mainly characterized by a C=O stretching, suggests that an explicit description of the water molecules is needed.

We now move to comment on the RREP, i.e. the Raman spectrum as a function of the external wavelength, of ACA in aqueous solution as calculated by means of QM/FQ (see Fig. 5. Note that an experimental RREP has been measured in Ref. 22. The excitation profiles of Amide I (C=O stretching), Amide II (NH_2 bending), Amide III (C-N stretching) as well as the CH_3 rocking vibration (1457 cm^{-1}) are reported in Figure 5(b). Two clear-cut trends can be seen in Figure 5(b): on one hand, similar to NMA, the amide I, II and III bands are resonance enhanced in ACA with Amides II and III increasing in intensity more than than Amide I. As expected, the enhancement is maximum facing 172 nm (see Sec. S2.3 in the SM), which is the computed QM/FQ excitation energy of the $\pi \rightarrow \pi^*$ transition (see Tab. S1 in the SM). As observed in Figure 5(b), this transition of the peptide group starts to be significant at excitation wavelengths near the maximum of the absorption curve, as reported in Ref. 22, where the authors found a relationship between the excitation wavelength and the Raman band positions for the same signals, associating it to the HB strength at the NH_2 and C=O sites.

5.3. DMA

5.3.1. Spontaneous Raman spectra

In Figure 6(a), the QM/PCM and QM/FQ spontaneous Raman spectra of DMA in aqueous solution are reported together with the measured experimental spectrum ($\omega_0 = 633$ nm). Overall, the Raman spectrum of DMA is dominated by the same amide bands previously mentioned for NMA and ACA (see also Sec. S3.1 in the SM). No significant differences between QM/PCM and QM/FQ solvation models can be noticed (Figure 6(a)). Both environmental treatments lead to peak positions close to the experimental ones, with the only exception being the Amide I band ($\sim 1650\ cm^{-1}$), for which QM/FQ also provide a more accurate prediction of its relative intensity. This is not unexpected because, as for the other two amides, Amide I band is largely affected by specific solute-solvent interactions.

5.3.2. UV Resonance Raman spectra

Simulated UVRR spectra of DMA in aqueous solution and experimental spectra, recorded using 226 nm as excitation wavelength, are depicted in Figure 6(b) (see also Fig. S14 in the SM). The overall picture that emerges from Figure 6(b) is of rather good agreement between theory and experiment, at least in terms of the major features. This overview is similar for both QM/PCM and QM/FQ models, even though a significant improvement is reached by QM/FQ, as judged by the description of the Amide I and Amide II, which occur at 1650 and 1490 cm^{-1}, respectively. This shows that a better description of the solute-solvent interactions, provided when the discrete water molecules are employed, is important also in this system but not as crucial as in the case of ACA and NMA, due to the presence of the two methyl groups. Small discrepancies between computed and experi-

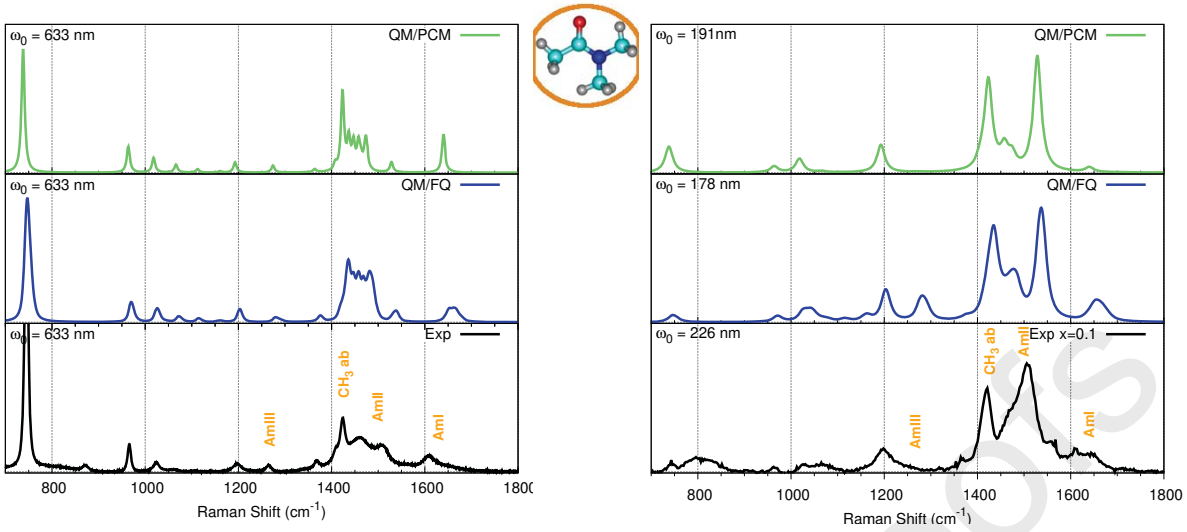

Figure 6: Raman spectra of **DMA** calculated with different solvent descriptions (top, QM/PCM and middle, QM/FQ) and compared to the experimental spectra (bottom) measured in aqueous solution at room temperature. (a) Spontaneous (Far From Resonance) Raman spectra simulated and measured using 633 nm as excitation wavelength. FWHM: 4 cm^{-1}. (b) UV Resonance Raman spectra. In the UVRR experiments, the external excitation wavelengths have been set to 226 nm. x=0.09 stands for the DMA molar fraction in water. RR intensities were calculated with a damping factor of 200 cm^{-1} and broadened using Lorentzian functions with a FWHM of 20 cm^{-1}. The RR band at around 800 cm^{-1} is a spurious signal arising from the quartz cuvette.

mental UVRR results can be explained considering that for DMA it has been reported that the amide bands are sensitive to changes in concentration.[78] Remarkably, in both solvation approaches, we are assuming an infinite dilute solution, which is not the case for experimental conditions.

The dependence of QM/FQ UVRR as a function of the excitation wavelength is reported in Fig. 7(a), whereas the enhancements of selected normal modes (Amide I, II, III and CH_3 antisymmetric bend) are illustrated in Fig. 7(b). An enhancement of the Amide II band relative to Amide I and Amide III is immediately perceived for excitation wavelengths nearby the absorption maximum (184 nm, see also Sec. S3.3 in the SM). Indeed, for this spectral region, Amide II band becomes five-fold more intense than both Amide I and Amide II bands. It is also clear from Figure 7(b) that the amide III band cross section shows essentially no resonance enhancement, differently from NMA and ACA, for which its intensity does change (see Figs 2(b) and 4(b)). Furthermore, by comparing our non–resonant (Figure 6(a)) and pre-resonant (Figure 6(b)) Raman results, we notice that the overcrowded region between 1400 and 1500 cm^{-1} turns into a couple of bands located at 1437 and 1487 cm^{-1}. For the first one, there is also an enhancement as incident light approaches λ_{max} as shown in Figure 7(b), middle panel.

6. Discussion

The results discussed in the previous sections clearly show that QM/FQ outperforms continuum solvation, and gives an almost perfect description of experimental UVRR spectra of all three amides. In this section, we discuss such findings on the basis of physico-chemical properties of the systems when dissolved in aqueous solution. In particular, the performance of the two solvation models in the description of both spontaneous and RR of ACA, NMA and DMA can be investigated by analyzing the resutls of MD simulations, which can provide a qualitative and quantitative overview on specific, directional solute-solvent interactions. To this end, in Fig. 8 we report the Spatial and Radial Distribution Functions (SDF and RDF, respectively), which were extracted from the last 10 ns of MD simulations. The two plots are complementary: RDFs are used to quantify the strength of HB interactions in terms of the average solute-solvent distance, whereas SDFs provide a graphical 3D depiction of the most favorable positions of water Hydrogen and Oxygen atoms.

From the inspection of Fig. 8 it is clear that the three amides can form strong HBs with the surrounding water molecules. Remarkably, SDFs show the importance of including virtual sites in the description of the solute's Oxygen atom, perfectly describing the directionality which characterizes HB interactions. For this reason, QM/FQ outperforms the implicit approximation (QM/PCM) in the description of Amide I and II bands, both involving the C=O bond, because the implicit approach lacks of any specific/directional interaction. In case of ACA and NMA, the importance of an atomistic description of the environment is also demonstrated by HB interactions which are established between the amide Hydrogen(s) and water molecules (see both RDFs and SDFs). The absence of the amide Hydrogen in DMA can explain the better agreement between QM/PCM and QM/FQ results. In fact, the NH group is involved in the most relevant vibrations in the studied region (700-1800 cm^{-1}). Nevertheless, also in this case, we highlight that a collection of configurations standing for the dynamical fluctuations of the solvent

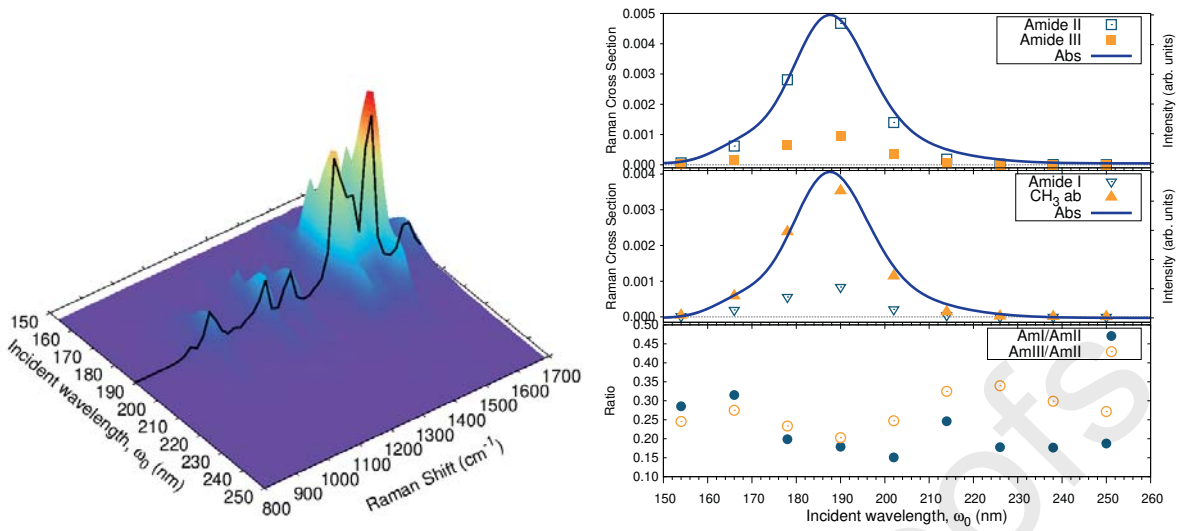

(a) (b)

Figure 7: (a) Calculated QM/FQ Resonance Raman Excitation Profile (RREP) of **DMA** in aqueous solution. (b) Excitation wavelength dependence of the Amide I, II, III and the 1430 cm^{-1} CCH_3 antisymmetric bend (ab) bands intensity, and of Amide I/Amide II and the Amide III/Amide II band Raman cross-section ratios. RR intensities (in $cm^2mol^{-1}sr^{-1}$) were broadened by a Lorentzian function with a FWHM of 20 cm^{-1} and a damping factor of 200 cm^{-1}.

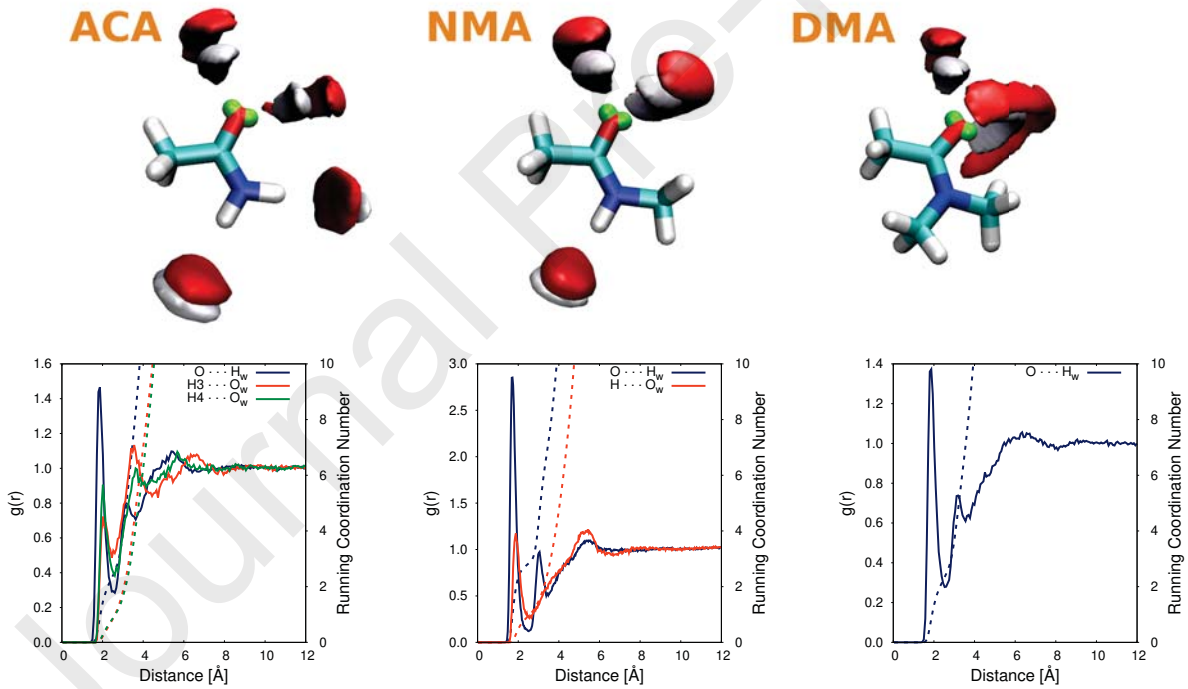

Figure 8: Top panel: SDFs for the three amides studied in this work. Calculated SDF isodensity values are equal to 70 and 80 nm^{-3} for water hydrogen (white surfaces) and oxygen (red surfaces) atoms, respectively. Bottom panel: Radial distribution function, *g(r)*, (solid lines) and running coordination numbers (dashed lines) for the hydrogen bonds CO···H_w and NH···O_w in the solvated amides.

molecules around the solute guarantees a much better agreement with experimental results.

To conclude, we note that the differences between QM/PCM and QM/FQ results are more pronounced for RR than for spontaneous Raman, thus confirming the necessity of an accurate and reliable description of solvation, as it is provided in this work by the coupling of the polarizable QM/FQ with classical MD simulations.

7. Summary and Conclusions

We have presented a joined computational and experimental work analyzing Raman and Resonance Raman (RR)

spectra of three simple amides, acetamide, *trans-N*-methyl acetamide and *N,N*-dimethyl acetamide, in aqueous solution. In particular, we focused on the effect that the aqueous environment induces on the spectra by comparing computational results obtained with the commonly employed continuum model and the polarizable QM/FQ approach, that permits to account for both polarization and specific hydrogen bonding effects. The study was also possible thanks to availability of SR-based UVRR experimental setup that allowed us to record accurate experimental spectra at low concentration of amides in water and with a variety of incident excitation wavelengths, an indispensable requirement for analyzing the effect of the resonant enhancement.

Our results demonstrate once again the severe shortcomings of the popular polarizable continuum model (PCM) in simulating the aqueous environment. In fact, Raman and RR spectra differ dramatically from their experimental counterpart at the PCM level, and the discrepancy is much more pronounced for systems having more potential sites for specific solute–solvent interactions. Being a mixed electronic and vibrational spectroscopy, RR requires an unbiased solvation model that is capable of capturing all solute-solvent interactions, and we have shown that our QM/FQ model gives highly accurate results. In fact, the agreement between theory and experiment is so high that the main features of the spectra are easily identified, in particular the assignment to the Amide I, Amide II and Amide III bands, that in primary amides (e.g. acetamide) are essentially due to C=O stretching, N–H bending and C–N stretching vibrations, respectively, while in secondary amides (e.g. NMA) the Amide II and III bands arise from combined N–H bending and C–N stretching vibrations. On the other hand, in tertiary amides (e.g. DMA), the lack of the amide hydrogen causes different contributions for Amide II and Amide III signals. Computed QM/FQ Resonance Raman Excitation Profiles (RREP) indicate that amide bands are particularly sensitive to variations in the incident wavelength, with the strongest changes occurring by approaching absorption spectra maxima, as earlier reported in experimental works.[19]

Given the success of the combination of theory and experiment in reproducing RR spectra of simple amides, the next step is to study more complex amino acids and peptides, which are essential building blocks of biological systems, and whose natural environment is water. The application of our method to these systems is in progress in our group, and will undoubtedly shed light into the complex mechanisms that cooperate to produce the final spectral response, thus building an understanding that is essential to and rationalize the spectroscopic features of complex protein systems.

Acknowledgements

SG and CC gratefully acknowledge the support of H2020-MSCA-ITN-2017 European Training Network "Computational Spectroscopy In Natural sciences and Engineering" (COSINE), grant number 765739. We gratefully acknowledge computational resources available at SNS Center for High Performance Computing (CHPC). We thank Dr. A. Gessini of the IUVS beamline at Elettra for the technical support.

A. Supplementary Material

Supplementary data associated with this article is available: NMA conformational analysis. NMA, ACA and DMA QM/FQ stick spectra and depiction of the normal modes. UVRR experimental spectra. NMA, ACA and DMA QM/FQ UV/Vis spectra.

References

[1] S. A. Asher, "Uv resonance raman studies of molecular structure and dynamics: Applications in physical and biophysical chemistry," *Annu. Rev. Phys. Chem.*, vol. 39, no. 1, pp. 537–588, 1988.

[2] S. A. Asher, "Uv resonance raman spectroscopy for analytical, physical, and biophysical chemistry. part 1," *Anal. Chem.*, vol. 65, no. 2, pp. 59A–66A, 1993.

[3] S. A. Asher, "Uv resonance raman spectroscopy for analytical, physical, and biophysical chemistry. part 2," *Anal. Chem.*, vol. 65, no. 4, pp. 201A–210A, 1993.

[4] K. Xiong, "Uv resonance raman spectroscopy: A highly sensitive, selective and fast technique for environmental analysis," *J. Environ. Anal. Chem*, vol. 2, no. 1, p. e107, 2014.

[5] Z. Chi and S. A. Asher, "Uv resonance raman determination of protein acid denaturation: Selective unfolding of helical segments of horse myoglobin," *Biochem.*, vol. 37, no. 9, pp. 2865–2872, 1998.

[6] Z. Ahmed, I. A. Beta, A. V. Mikhonin, and S. A. Asher, "Uv–resonance raman thermal unfolding study of trp-cage shows that it is not a simple two-state miniprotein," *J. Am. Chem. Soc.*, vol. 127, no. 31, pp. 10943–10950, 2005.

[7] C.-Y. Huang, G. Balakrishnan, and T. G. Spiro, "Early events in apomyoglobin unfolding probed by laser t-jump/uv resonance raman spectroscopy," *Biochem.*, vol. 44, no. 48, pp. 15734–15742, 2005.

[8] X. Zhao, R. Chen, C. Tengroth, and T. G. Spiro, "Solid-state tunable khz ultraviolet laser for raman applications," *Appl. Spectrosc.*, vol. 53, no. 10, pp. 1200–1205, 1999.

[9] A. V. Mikhonin and S. A. Asher, "Uncoupled peptide bond vibrations in α-helical and polyproline ii conformations of polyalanine peptides," *J. Phys. Chem. B*, vol. 109, no. 7, pp. 3047–3052, 2005.

[10] G. Balakrishnan, Y. Hu, G. M. Bender, Z. Getahun, W. F. DeGrado, and T. G. Spiro, "Enthalpic and entropic stages in α-helical peptide unfolding, from laser t-jump/uv raman spectroscopy," *J. Am. Chem. Soc.*, vol. 129, no. 42, pp. 12801–12808, 2007.

[11] S. Catalini, B. Rossi, P. Foggi, C. Masciovecchio, and F. Bruni, "Aqueous solvation of glutathione probed by uv resonance raman spectroscopy," *J. Mol. Liq.*, vol. 283, pp. 537–547, 2019.

[12] K. Kaya and S. Nagakura, "Electronic absorption spectra of hydrogen bonded amides," *Theor. Chim. Acta*, vol. 7, pp. 124–132, Apr 1967.

[13] J. M. Dudik, C. R. Johnson, and S. A. Asher, "Uv resonance raman studies of acetone, acetamide, and n-methylacetamide: models for the peptide bond," *J. Phys. Chem.*, vol. 89, no. 18, pp. 3805–3814, 1985.

[14] L. C. Mayne and B. Hudson, "Resonance raman spectroscopy of n-methylacetamide: overtones and combinations of the carbon-nitrogen stretch (amide ii') and effect of solvation on the carbon-oxygen double-bond stretch (amide i) intensity," *J. Phys. Chem.*, vol. 95, no. 8, pp. 2962–2967, 1991.

[15] X. G. Chen, R. Schweitzer-Stenner, S. Krimm, N. G. Mirkin, and S. A. Asher, "N-methylacetamide and its hydrogen-bonded water molecules are vibrationally coupled," *J. Am. Chem. Soc.*, vol. 116, no. 24, pp. 11141–11142, 1994.

[16] X. G. Chen, R. Schweitzer-Stenner, S. A. Asher, N. G. Mirkin, and S. Krimm, "Vibrational assignments of trans-n-methylacetamide and some of its deuterated isotopomers from band decomposition of ir,

visible, and resonance raman spectra," *J. Phys. Chem.*, vol. 99, no. 10, pp. 3074–3083, 1995.

[17] X. G. Chen, S. A. Asher, R. Schweitzer-Stenner, N. G. Mirkin, and S. Krimm, "Uv raman determination of the .pi..pi.* excited state geometry of n-methylacetamide: Vibrational enhancement pattern," *J. Am. Chem. Soc.*, vol. 117, no. 10, pp. 2884–2895, 1995.

[18] B. Rossi, S. Catalini, C. Bottari, A. Gessini, and C. Masciovecchio, "Frontiers of UV resonant raman spectroscopy by using synchrotron radiation: the case of aqueous solvation of model peptides," in *UV and Higher Energy Photonics: From Materials to Applications 2019* (G. Lérondel, Y.-H. Cho, A. Taguchi, and S. Kawata, eds.), vol. 11086, pp. 23 – 32, International Society for Optics and Photonics, SPIE, 2019.

[19] F. D'Amico, B. Rossi, G. Camisasca, F. Bencivenga, A. Gessini, E. Principi, R. Cucini, and C. Masciovecchio, "Slow-to-fast transition of hydrogen bond dynamics in acetamide hydration shell formation," *Phys. Chem. Chem. Phys.*, vol. 17, pp. 10987–10992, 2015.

[20] Q. Wu, G. Balakrishnan, A. Pevsner, and T. G. Spiro, "Histidine photodegradation during uv resonance raman spectroscopy," *J. Phys. Chem. A*, vol. 107, no. 40, pp. 8047–8051, 2003.

[21] J. Kneipp, G. Balakrishnan, R. Chen, T.-J. Shen, S. C. Sahu, N. T. Ho, J. L. Giovannelli, V. Simplaceanu, C. Ho, and T. G. Spiro, "Dynamics of allostery in hemoglobin: Roles of the penultimate tyrosine h bonds," *J. Mol. Biol.*, vol. 356, no. 2, pp. 335 – 353, 2006.

[22] M. Saito, F. D'Amico, G. Camisasca, F. Bencivenga, R. Cucini, A. Gessini, E. Principi, T. Ogura, and C. Masciovecchio, "Resonance raman spectroscopy with chemical state selectivity on histidine and acetamide using synchrotron radiation," *Bull. Chem. Soc. Jpn.*, vol. 88, no. 4, pp. 591–596, 2015.

[23] S. P. Fodor and T. G. Spiro, "Ultraviolet resonance raman spectroscopy of dna with 200-266-nm laser excitation," *J. Am. Chem. Soc.*, vol. 108, no. 12, pp. 3198–3205, 1986.

[24] S. Ng, S. Yarasi, P. Brost, and G. R. Loppnow, "Initial excited-state structural dynamics of thymine are coincident with the expected photochemical dynamics," *J. Phys. Chem. A*, vol. 112, no. 41, pp. 10436–10437, 2008.

[25] S. Yarasi, S. Ng, and G. R. Loppnow, "Initial excited-state structural dynamics of uracil from resonance raman spectroscopy are different from those of thymine (5-methyluracil)," *J. Phys. Chem. B*, vol. 113, no. 43, pp. 14336–14342, 2009.

[26] F. Bianchi, L. Comez, R. Biehl, F. D'Amico, A. Gessini, M. Longo, C. Masciovecchio, C. Petrillo, A. Radulescu, B. Rossi, F. Sacchetti, F. Sebastiani, N. Violini, and A. Paciaroni, "Structure of human telomere G-quadruplex in the presence of a model drug along the thermal unfolding pathway," *Nucleic Acids Res.*, vol. 46, pp. 11927–11938, 11 2018.

[27] C. Bottari, S. Catalini, P. Foggi, I. Mancini, A. Mele, D. R. Perinelli, A. Paciaroni, A. Gessini, C. Masciovecchio, and B. Rossi, "Base-specific pre-melting and melting transitions of dna in presence of ionic liquids probed by synchrotron-based uv resonance raman scattering," *J. Mol. Liq.*, vol. 330, p. 115433, 2021.

[28] A. Ianoul, T. Coleman, and S. A. Asher, "Uv resonance raman spectroscopic detection of nitrate and nitrite in wastewater treatment processes," *Anal. Chem.*, vol. 74, no. 6, pp. 1458–1461, 2002.

[29] D. D. Tuschel, A. V. Mikhonin, B. E. Lemoff, and S. A. Asher, "Deep ultraviolet resonance raman excitation enables explosives detection," *Appl. Spectrosc.*, vol. 64, no. 4, pp. 425–432, 2010.

[30] S. A. Oladepo, K. Xiong, Z. Hong, and S. A. Asher, "Elucidating peptide and protein structure and dynamics: Uv resonance raman spectroscopy," *J. Phys. Chem. Lett.*, vol. 2, no. 4, pp. 334–344, 2011.

[31] M. S. Barclay, T. J. Quincy, D. B. Williams-Young, M. Caricato, and C. G. Elles, "Accurate assignments of excited-state resonance raman spectra: A benchmark study combining experiment and theory," *J. Phys. Chem. A*, vol. 121, no. 41, pp. 7937–7946, 2017.

[32] C. R. Johnson and S. A. Asher, "A new selective technique for characterization of polycyclic aromatic hydrocarbons in complex samples: Uv resonance raman spectrometry of coal liquids," *Anal. Chem.*, vol. 56, no. 12, pp. 2258–2261, 1984.

[33] S. A. Asher, "Ultraviolet resonance raman spectrometry for detection and speciation of trace polycyclic aromatic hydrocarbons," *Anal. Chem.*, vol. 56, no. 4, pp. 720–724, 1984.

[34] D. A. Long, *Vibrational Resonance Raman Scattering*, ch. 7, pp. 221–270. John Wiley & Sons, Ltd, 2002.

[35] Y. Ozaki *et al.*, *Molecular Spectroscopy: A Quantum Chemistry Approach*. John Wiley & Sons, 2019.

[36] S. Bykov, I. Lednev, A. Ianoul, A. Mikhonin, C. Munro, and S. A. Asher, "Steady-state and transient ultraviolet resonance raman spectrometer for the 193–270 nm spectral region," *Appl. Spectrosc.*, vol. 59, pp. 1541–1552, Dec 2005.

[37] B. Rossi, C. Bottari, S. Catalini, F. D'Amico, A. Gessini, and C. Masciovecchio, "Chapter 13 - synchrotron-based ultraviolet resonance raman scattering for material science," in *Molecular and Laser Spectroscopy* (V. Gupta and Y. Ozaki, eds.), pp. 447–482, Elsevier, 2020.

[38] F. Egidi, J. Bloino, C. Cappelli, and V. Barone, "A robust and effective time-independent route to the calculation of resonance raman spectra of large molecules in condensed phases with the inclusion of duschinsky, herzberg–teller, anharmonic, and environmental effects," *J. Chem. Theory Comput.*, vol. 10, no. 1, pp. 346–363, 2014.

[39] F. J. Avila Ferrer, V. Barone, C. Cappelli, and F. Santoro, "Duschinsky, herzberg–teller, and multiple electronic resonance interferential effects in resonance raman spectra and excitation profiles. the case of pyrene," *J. Chem. Theory Comput.*, vol. 9, no. 8, pp. 3597–3611, 2013.

[40] F. Santoro, C. Cappelli, and V. Barone, "Effective time-independent calculations of vibrational resonance raman spectra of isolated and solvated molecules including duschinsky and herzberg–teller effects," *J. Chem. Theory Comput.*, vol. 7, no. 6, pp. 1824–1839, 2011.

[41] B. Mennucci, "Polarizable continuum model," *WIREs Comput Mol Sci.*, vol. 2, no. 3, pp. 386–404, 2012.

[42] A. Baiardi, J. Bloino, and V. Barone, "A general time-dependent route to resonance-raman spectroscopy including franck-condon, herzberg-teller and duschinsky effects," *J. Chem. Phys.*, vol. 141, no. 11, p. 114108, 2014.

[43] L. M. Markham and B. S. Hudson, "Ab initio analysis of the effects of aqueous solvation on the resonance raman intensities of n-methylacetamide," *J. Phys. Chem.*, vol. 100, no. 7, pp. 2731–2737, 1996.

[44] N. S. Myshakina, Z. Ahmed, and S. A. Asher, "Dependence of amide vibrations on hydrogen bonding," *J. Phys. Chem. B*, vol. 112, no. 38, pp. 11873–11877, 2008.

[45] H. M. Senn and W. Thiel, "QM/MM methods for biomolecular systems," *Angew. Chem. Int. Ed.*, vol. 48, no. 7, pp. 1198–1229, 2009.

[46] U. N. Morzan, D. J. Alonso de Armiño, N. O. Foglia, F. Ramírez, M. C. González Lebrero, D. A. Scherlis, and D. A. Estrin, "Spectroscopy in complex environments from qm–mm simulations," *Chem. Rev.*, vol. 118, no. 7, pp. 4071–4113, 2018.

[47] H. Ren, J. Jiang, and S. Mukamel, "Deep uv resonance raman spectroscopy of β-sheet amyloid fibrils: A qm/mm simulation," *J. Phys. Chem. B*, vol. 115, no. 47, pp. 13955–13962, 2011.

[48] V. Macaluso, L. Cupellini, G. Salvadori, F. Lipparini, and B. Mennucci, "Elucidating the role of structural fluctuations, and intermolecular and vibronic interactions in the spectroscopic response of a bacteriophytochrome," *Phys. Chem. Chem. Phys.*, vol. 22, pp. 8585–8594, 2020.

[49] T. Giovannini, F. Egidi, and C. Cappelli, "Molecular spectroscopy of aqueous solutions: a theoretical perspective," *Chem. Soc. Rev.*, vol. 49, pp. 5664–5677, 2020.

[50] C. Cappelli, "Integrated qm/polarizable mm/continuum approaches to model chiroptical properties of strongly interacting solute–solvent systems," *Int. J. Quant. Chem.*, vol. 116, no. 21, pp. 1532–1542, 2016.

[51] T. Giovannini, F. Egidi, and C. Cappelli, "Theory and algorithms for chiroptical properties and spectroscopies of aqueous systems," *Phys. Chem. Chem. Phys.*, vol. 22, pp. 22864–22879, 2020.

[52] L. Jensen, L. L. Zhao, J. Autschbach, and G. C. Schatz, "Theory and method for calculating resonance raman scattering from resonance polarizability derivatives," *J. Chem. Phys.*, vol. 123, no. 17,

p. 174110, 2005.
[53] E. J. Heller, R. Sundberg, and D. Tannor, "Simple aspects of raman scattering," *J. Phys. Chem.*, vol. 86, no. 10, pp. 1822–1833, 1982.
[54] D. J. Tannor and E. J. Heller, "Polyatomic raman scattering for general harmonic potentials," *J. Chem. Phys.*, vol. 77, no. 1, pp. 202–218, 1982.
[55] A. B. Myers, "Resonance raman intensity analysis of excited-state dynamics," *Acc. Chem. Res.*, vol. 30, no. 12, pp. 519–527, 1997.
[56] G. N. R. Tripathi, "Electronic structure of para aminophenoxyl radical in water," *J. Chem. Phys.*, vol. 118, no. 3, pp. 1378–1391, 2003.
[57] J. Guthmuller and B. Champagne, "Time dependent density functional theory investigation of the resonance raman properties of the julolidinemalononitrile push-pull chromophore in various solvents," *J. Chem. Phys.*, vol. 127, no. 16, p. 164507, 2007.
[58] J. Guthmuller, "Comparison of simplified sum-over-state expressions to calculate resonance raman intensities including franck-condon and herzberg-teller effects," *J. Chem. Phys.*, vol. 144, no. 6, p. 064106, 2016.
[59] T. Giovannini, M. Olszówka, F. Egidi, J. R. Cheeseman, G. Scalmani, and C. Cappelli, "Polarizable embedding approach for the analytical calculation of raman and raman optical activity spectra of solvated systems," *J. Chem. Theory Comput.*, vol. 13, no. 9, pp. 4421–4435, 2017.
[60] F. Lipparini, C. Cappelli, and V. Barone, "Linear response theory and electronic transition energies for a fully polarizable QM/classical hamiltonian," *J. Chem. Theory Comput.*, vol. 8, no. 11, pp. 4153–4165, 2012.
[61] I. Carnimeo, C. Cappelli, and V. Barone, "Analytical gradients for mp2, double hybrid functionals, and td-dft with polarizable embedding described by fluctuating charges," *J. Comput. Chem.*, vol. 36, no. 31, pp. 2271–2290, 2015.
[62] M. J. Frisch, G. W. Trucks, H. B. Schlegel, G. E. Scuseria, M. A. Robb, J. R. Cheeseman, G. Scalmani, and et al, "Gaussian 16 Revision A.03," 2016. Gaussian Inc. Wallingford CT.
[63] A. V. Marenich, S. V. Jerome, C. J. Cramer, and D. G. Truhlar, "Charge model 5: An extension of hirshfeld population analysis for the accurate description of molecular interactions in gaseous and condensed phases," *J. Chem. Theory Comput.*, vol. 8, no. 2, pp. 527–541, 2012.
[64] M. J. Abrahama, T. Murtola, R. Schulz, S. Pálla, J. C. Smith, B. Hess, and E. Lindahl, "GROMACS: High performance molecular simulations through multi-level parallelism from laptops to supercomputers," *SoftwareX*, vol. 1-2, pp. 19–25, 2015.
[65] M. Macchiagodena, G. Mancini, M. Pagliai, and V. Barone, "Accurate prediction of bulk properties in hydrogen bonded liquids: Amides as case studies," *Phys. Chem. Chem. Phys.*, vol. 18, pp. 25342–25354, 2016.
[66] M. Macchiagodena, G. Mancini, M. Pagliai, G. Del Frate, and V. Barone, "Fine-tuning of atomic point charges: Classical simulations of pyridine in different environments," *Chem. Phys. Lett.*, vol. 677, pp. 120–126, 2017.
[67] T. Giovannini, M. Macchiagodena, M. Ambrosetti, A. Puglisi, P. Lafiosca, G. Lo Gerfo, F. Egidi, and C. Cappelli, "Simulating vertical excitation energies of solvated dyes: From continuum to polarizable discrete modeling," *Int. J. Quant. Chem.*, vol. 119, no. 1, p. e25684, 2019.
[68] A. Puglisi, T. Giovannini, L. Antonov, and C. Cappelli, "Interplay between conformational and solvent effects in uv-visible absorption spectra: curcumin tautomers as a case study," *Phys. Chem. Chem. Phys.*, vol. 21, pp. 15504–15514, 2019.
[69] T. Giovannini, M. Ambrosetti, and C. Cappelli, "A polarizable embedding approach to second harmonic generation (shg) of molecular systems in aqueous solutions," *Theor. Chem. Acc.*, vol. 137, p. 74, May 2018.
[70] S. F. Boys, "Construction of some molecular orbitals to be approximately invariant for changes from one molecule to another," *Rev. Mod. Phys.*, vol. 32, pp. 296–299, 1960.
[71] J. Wang, R. M. Wolf, J. W. Caldwell, P. A. Kollman, and D. A. Case, "Development and testing of a general amber force field," *J. Comput. Chem.*, vol. 25, no. 9, pp. 1157–1174, 2004.
[72] G. Bussi, D. Donadio, and M. Parrinello, "Canonical sampling through velocity rescaling," *J. Chem. Phys.*, vol. 126, no. 1, p. 014101, 2007.
[73] M. Brehm and B. Kirchner, "Travis - a free analyzer and visualizer for monte carlo and molecular dynamics trajectories," *J. Chem. Inf. Model.*, vol. 51, no. 8, pp. 2007–2023, 2011.
[74] X. Li and M. J. Frisch, "Energy-represented direct inversion in the iterative subspace within a hybrid geometry optimization method," *J. Chem. Theory Comput.*, vol. 2, no. 3, pp. 835–839, 2006.
[75] S. W. Rick, S. J. Stuart, and B. J. Berne, "Dynamical fluctuating charge force fields: Application to liquid water," *J. Chem. Phys.*, vol. 101, no. 7, pp. 6141–6156, 1994.
[76] S. A. Asher, Z. Chi, and P. Li, "Resonance Raman examination of the two lowest amide $\pi\pi^*$ excited states," *J. Raman Spectrosc.*, vol. 29, no. 10-11, pp. 927–931, 1998.
[77] D. Punihaole, R. S. Jakubek, E. M. Dahlburg, Z. Hong, N. S. Myshakina, S. Geib, and S. A. Asher, "Uv resonance raman investigation of the aqueous solvation dependence of primary amide vibrations," *J. Phys. Chem. B*, vol. 119, no. 10, pp. 3931–3939, 2015.
[78] N. E. Triggs and J. J. Valentini, "An investigation of hydrogen bonding in amides using raman spectroscopy," *J. Phys. Chem.*, vol. 96, no. 17, pp. 6922–6931, 1992.
[79] T. Giovannini, M. Olszówka, and C. Cappelli, "Effective fully polarizable qm/mm approach to model vibrational circular dichroism spectra of systems in aqueous solution," *J. Chem. Theory Comput.*, vol. 12, no. 11, pp. 5483–5492, 2016.
[80] T. Giovannini, G. Del Frate, P. Lafiosca, and C. Cappelli, "Effective computational route towards vibrational optical activity spectra of chiral molecules in aqueous solution," *Phys. Chem. Chem. Phys.*, vol. 20, pp. 9181–9197, 2018.

Journal Pre-proofs